

CrystEngComm

Accepted Manuscript



This is an *Accepted Manuscript*, which has been through the Royal Society of Chemistry peer review process and has been accepted for publication.

Accepted Manuscripts are published online shortly after acceptance, before technical editing, formatting and proof reading. Using this free service, authors can make their results available to the community, in citable form, before we publish the edited article. We will replace this *Accepted Manuscript* with the edited and formatted *Advance Article* as soon as it is available.

You can find more information about *Accepted Manuscripts* in the [Information for Authors](#).

Please note that technical editing may introduce minor changes to the text and/or graphics, which may alter content. The journal's standard [Terms & Conditions](#) and the [Ethical guidelines](#) still apply. In no event shall the Royal Society of Chemistry be held responsible for any errors or omissions in this *Accepted Manuscript* or any consequences arising from the use of any information it contains.

PAPER

Conformal growth of copper sulfide thin films on highly textured surface *via* a microreactor-assisted solution deposition

Paravee Vas-Umnuay,^{†ac} Ki-Joong Kim,^{†a} Dae-Hwan Kim^b and Chih-Hung Chang^{*a}

Cite this: DOI: 10.1039/x0xx00000x

Received 00th January 2012,
Accepted 00th January 2012

DOI: 10.1039/x0xx00000x

www.rsc.org/

In this work, the preparation of copper sulfide (Cu_xS) thin films *via* microreactor-assisted solution deposition (MASD), where separation of the homogeneous reaction and deposition from the molecular level heterogeneous surface reaction is demonstrated. A particle-free flux in solution was obtained by adjusting the key process parameters, namely concentration of reactants, reaction temperature, and residence time, resulting a high quality film and a high deposition rate (40 - 100 times higher than that of deposited by chemical bath deposition). Moreover, the growth of Cu_xS thin films was monitored using an *in-situ* quartz crystal microbalance. We found that the growth rate significantly depends on the heterogeneous temperature and residence time, while limited influence of homogeneous temperature was observed. Furthermore, conformal and dense Cu_xS thin films were deposited on a highly textured Si surface that demonstrates enhanced photon absorption.

Introduction

The use of structured substrates opens an avenue to increase photon absorption in the absorber layer of solar photovoltaic devices. This can lead to the more efficient use of solar absorber materials and more advanced solar cell designs. There have been many prior studies demonstrating that nanoscale texturing can increase light absorption in thin-film solar cells.¹⁻³ For example, Jeong *et al.* demonstrated that amorphous silicon thin films deposited on silica nanoparticle monolayers exhibit 42 % higher absorption than planar controls.⁴ Increased absorption efficiency also enables the concept of extremely thin absorber solar cells, based on sandwiching a thin semiconductor solar absorber between two transparent, highly structured p and n-type semiconductors.^{5,6} The ability to achieve conformal growth of high quality thin films is needed for these novel approaches.

Copper sulfides (Cu_xS), the focus of this work, are some of the most attractive metal chalcogenide semiconductors due to their wide range of applications in electrical and optical devices, such as solar control coatings, photothermal conversion, solar cells, and microwave shielding coatings.⁷⁻¹³ Cu_xS is also an important binary precursor that could lead to the formations of $\text{Cu}_2\text{ZnSn}(\text{S},\text{Se})_4$ thin film solar cells *via* a stacked layer approach.¹⁴ Cu_xS is a p-type material due to the copper

vacancies in the lattice, with the optical band gap ranging from 1.2 eV - 2.5 eV depending on the value of x between 1 and 2. At room temperature, five stable phases of Cu_xS are known to exist in the bulk form: CuS (covellite), $\text{Cu}_{1.75}\text{S}$ (anilite), $\text{Cu}_{1.8}\text{S}$ (digenite), $\text{Cu}_{1.96}\text{S}$ (djurleite), and Cu_2S (chalcocite).^{15,16}

Among these materials, covellite CuS thin films exhibit metal-like electrical conductivity and possess near-ideal solar control characteristics¹⁷ due to a broad absorption spectrums in both visible and near-infrared regions, and thus covellite is a promising material in the field of photocatalysis,¹⁸ solar cells,¹⁹ and as a precursor for CIGS and CZTS solar cells.

Several approaches have been reported to prepare high quality and uniform Cu_xS thin films, including spray pyrolysis,¹¹ chemical vapor deposition,²⁰ successive ionic layer adsorption and reaction,²¹ and photochemical deposition.²² However, these deposition techniques generally require complex equipment and are consequently costly to implement on a large scale. In contrast, solution-based deposition routes, such as colloidal nanoparticle-based²³⁻²⁵ and CBD methods, can provide low-cost, scalable synthetic routes. Although the colloidal nanoparticle-based methods are ideal for making nanocomposite films,²⁶⁻²⁸ they are not suitable for the preparation of uniform and conformal coatings over highly textured substrates. Furthermore, the colloidal nanoparticle-

based route for thin film formation normally requires a high-temperature annealing step to remove the organic ligands.

Low-temperature chemical bath deposition (CBD)^{7,9,29-31} has been developed as the simplest technique and was widely investigated in the growth of Cu_xS thin films because of low-cost and ability to accurately control film composition. One problem with the CBD process is the generation of solid particles due to supersaturation in the reaction bath, leading to non-linear growth rates and poor elucidation of the reaction mechanism. To overcome this issue, the continuous flow microreactor-assisted solution deposition (MASD) process system has been developed. This technique allows for better understanding of the reaction mechanism by separating the homogeneous particle formation and deposition from the heterogeneous surface reaction, which resulted in improved quality and uniformity of the thin films.³²⁻³⁴ In addition, the total deposition time is relatively short compared CBD process. MASD has successfully applied a particle-free flux of CdS by controlling the residence time, leading to better surface coverage and uniformity of CdS films on SiO₂/Si substrates in comparison with the conventional CBD process.³⁵ Mugdur *et al.* was also able to obtain a reacting flux without the formation of nanoparticles at a very short residence time of a few seconds for deposition of CdS thin films,^{32,36} and they elucidated the growth kinetics and mechanism of CdS film growth.

Herein, we demonstrate the MASD process combined with the homogeneous reaction *via* the particle-free flux and the heterogeneous reaction by controlling the temperature of the solution, the concentration of mixed reactants, and the residence time. In addition, the kinetic study of Cu_xS film growth under various deposition conditions was investigated using an *in-situ* technique and the growth mechanism of Cu_xS thin films was also proposed based on experimental observations. With demonstrated MASD system, conformal and uniform thin Cu_xS films were able to grow on a highly textured silicon surface that would expect enhanced photon absorption in comparison with the same film on a flat surface.

Experimental

Deposition of Cu_xS thin films

Microscope glass slides (0.5 in. × 0.5 in.) were used as a substrate for the Cu_xS deposition. Initially glass slides were cleaned with a commercial detergent solution by scrubbing followed by acetone, methanol, and deionized (DI) water. Finally clean substrates were dried in flowing N₂ gas before use for the deposition.

The MASD system consists of a peristaltic pump, micromixer, constant temperature bath, and hot-plate with a temperature controller, as shown in Fig. 1(A). The reactants in streams A and B were initially pumped into the Tygon tubing individually and allowed to mix through a micromixer. Based on the formulation of Cu_xS thin films deposited by CBD,¹⁸ the final concentration of each reactant in the solution bath consists

of copper sulfate [CuSO₄] = 0.02 M, sodium acetate [NaAc] = 0.02 M, triethanolamine [TEA] = 0.151 M, ammonia [NH₃] = 0.164 M, and thiourea [SC(NH₂)₂] = 0.011 M, resulting in the ratio of [CuSO₄] : [NaAc] : [TEA] : [NH₄OH] : [SC(NH₂)₂] = 1 : 1 : 7.55 : 8.21 : 0.56. The resulting mixture from the micromixer was then passed through PEEK tubing (0.04 in. ID and 10.43 in. long), which was enclosed coaxially in a tygon tube, serving as a shell and tube heat exchanger with hot water circulation by a constant temperature bath. The solution was impinged onto the glass substrate, which was taped on the metallic plate heated on a hot plate. Once the process was completed, the substrate was removed, washed with DI water several times, and dried under a stream of N₂ gas. The variation of experimental conditions is summarized in Table 1.

In-situ growth measurement of Cu_xS thin films

The growth kinetics of deposited Cu_xS thin films under the variation of reaction conditions were measured using a quartz crystal microbalance (QCM, Maxtek) operating at a frequency of 5 MHz gold. The QCM flow cell system with an inlet and outlet was used for the continuous deposition process, as shown in Fig. 1(B). The setup consisted of a QCM flow cell probe with a quartz crystal inserted inside and immersed in the water bath to control the temperature. The signal from the quartz crystal probe is sent to the quartz crystal monitor and computer for data acquisition.

Formation of textured pyramidal Si substrate

Polished silicon (100) wafers as substrate was rinsed with detergent and dried with the flow of N₂ gas. The substrate was emerged into 2 vol.% of isopropyl alcohol in 0.5 M of sodium hydroxide at 80 °C for 30 min with vigorous stirring. The textured pyramidal surface of Si substrate was then rinsed with DI water, diluted HCl, and DI water again. Finally, the sample was dried by a stream of N₂ gas.

Characterization of Cu_xS thin films

The surface morphology and composition of Cu_xS thin films were characterized by scanning electron microscopy (SEM, Quanta 600 FEG) coupled with the energy dispersive X-ray spectroscopy (EDS). Transmission electron microscopy (TEM, Philips CM12 STEM) was used to study the particle formation on a substrate. TEM grids were placed on the hotplate, heated at corresponding conditions temperature, and rinsed with DI water and dried after the deposition. The optical properties were determined using ultraviolet-visible-near infrared spectrophotometry (UV-Vis-NIR, JASCO V670). Raman spectra were recorded using a WITec confocal Raman microscope with a 532.4 nm of wavelength and CCD detector. X-ray diffraction patterns were obtained using a Rigaku Ultima IV Diffractometer, operating at 40 kV and 40 mA with Cu *ka* radiation (0.154 nm). X-ray photoelectron spectroscopy (XPS) spectra were acquired with an ESCALAB 250 (Thermo Scientific) by using a microfocussed (500 μm, 157 W) Al K_α X-ray beam. The binding energies were calibrated using the C 1s signal located at 284.5 eV.

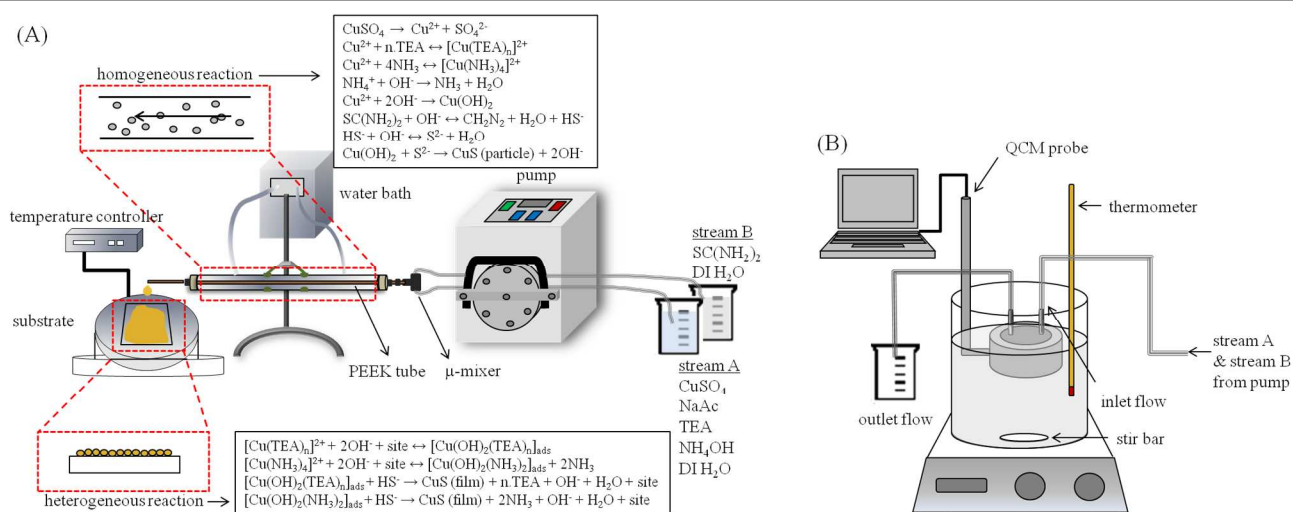


Fig. 1. (A) Schematic diagram of the MASD system and (B) schematic diagram of *in-situ* QCM flow cell setup for kinetic study.

Table 1 Summary of experimental conditions in MASD system

Entry	Parameters	Concentration of $\text{CuSO}_4 : \text{NaAc} : \text{TEA} : \text{NH}_3 : \text{SC}(\text{NH}_2)_2$ (mol) ^a	Residence time (sec) ^b	T_{homo} ($^{\circ}\text{C}$) ^c	T_{het} ($^{\circ}\text{C}$) ^d	Deposition time (sec) ^e
1			62	40	40	
2		0.10 : 0.10 : 0.755 : 0.822 : 0.0560	104	40	40	One drop ^f
3			125	40	40	
4			125	40	40	10
5	Effect of concentration of mixed reactant	0.05 : 0.05 : 0.375 : 0.411 : 0.0278	125	40	40	30
6			125	40	40	50
7			125	40	40	75
8			62	25	80	10
9		0.02 : 0.02 : 0.151 : 0.164 : 0.0110	62	25	80	20
10			62	25	80	30
11			62	25	80	0 - 2100
12	Effect of residence time	0.02 : 0.02 : 0.151 : 0.164 : 0.0110	84	25	80	0 - 2100
13			125	25	80	0 - 2100
14			125	25	40	0 - 2100
15	Effect of temperature at homogeneous reaction	0.02 : 0.02 : 0.151 : 0.164 : 0.0110	125	30	40	0 - 2100
16			125	40	40	0 - 2100
17			62	25	60	0 - 2100
18	Effect of temperature at heterogeneous reaction	0.02 : 0.02 : 0.151 : 0.164 : 0.0110	62	25	70	0 - 2100
19			62	25	80	0 - 2100
20			62	25	90	0 - 2100
21			62	25	80	60
22	Effect of deposition time	0.02 : 0.02 : 0.151 : 0.164 : 0.0110	62	25	80	120
23			62	25	80	240

^aConcentrations of mixed reactants. ^bResidence times of homogeneous reaction zone. ^cTemperatures of homogeneous reaction zone. ^dTemperatures of heterogeneous reaction zone. ^eDeposition time onto TEM grid or QCM surface. ^fCollection of one drop of solution onto TEM grid.

Results and discussion

Investigation of Cu_xS nanoparticle formation in the solution (Entries 1 - 10)

The preliminary study was to investigate a particle-free flux in the homogeneous reaction before the reactant solution impinges on the substrate. The homogeneous temperature (T_{homo}) was first set to 40 $^{\circ}\text{C}$ and the heterogeneous temperature (T_{het}) of TEM grid was maintained at 40 $^{\circ}\text{C}$. The residence time was varied from 62 s to 125 s (Entries 1 - 3 in Table 1). Fig. 2(A) shows that a large number of the nanoparticles were observed at the long residence time, and

decreases in number of the nanoparticles were obtained at shorter residence times (Fig. 2(B) - 2(C)). However, the results show that the particles formation could not be completely avoided even with short residence time. Further decreasing either homogeneous or heterogeneous temperature at this concentration could not obtain the uniform thin films (data not shown).

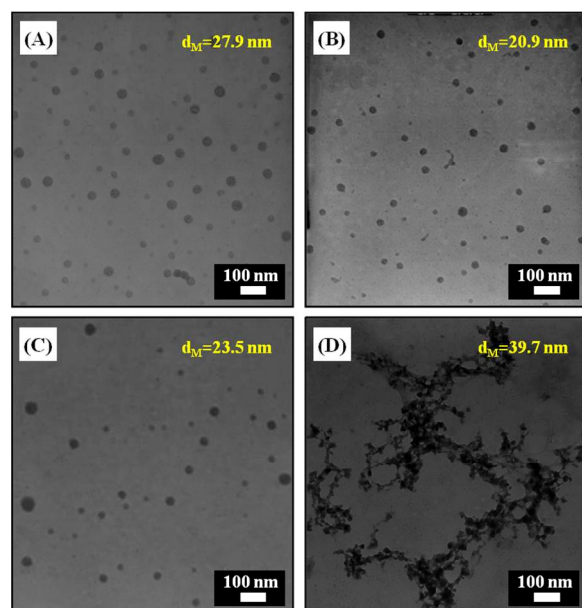


Fig. 2. TEM micrographs of Cu_xS nanoparticles collected from homogeneous reaction at $T_{\text{homo}} = 40\text{ }^\circ\text{C}$, $T_{\text{het}} = 40\text{ }^\circ\text{C}$, and at the residence times of (A) 125 s (Entry 3), (B) 104 s (Entry 2), and (C) 62 s (Entry 1). (D) TEM micrograph of Cu_xS film collected from homogeneous reaction (Entry 4). All images are included with the particle size histograms.

In order to obtain a particle-free flux in the homogeneous reaction flow, the concentration of precursors was decreased by a factor of two, as shown in Entries 4 - 7 in Table 1. We found that the minimum residence time of 125 s, and homogeneous and heterogeneous temperatures of $40\text{ }^\circ\text{C}$ produced the most uniform and continuous Cu_xS films. Fig. 3 show the TEM images for the deposition times of 10 s (A), 30 s (B), 50 s (C), and 75 s (D). It is clearly seen that uniform nanoparticles of 20 nm - 30 nm were obtained from deposition time of 10 s. The particle sizes slightly increase to about 40 nm at 30 s, as shown in Fig. 3(B). The corresponding electron diffraction pattern shown in Fig. 3(B) reveals the nanocrystalline state. At 50 s, another layer of nanoparticle formation appears on top of the lower layer ((Fig. 3(C)). This observation could be attributed to the secondary nucleation occurring in the presence of a solute-particle interface which is induced by crystals. Nanoparticles continue to grow and cover the substrate completely at the deposition time of 75 s, as shown in Fig. 3(D). The inset image also demonstrates an increase in sizes of large particles aggregating from homogeneous reaction the substrate. It was noted that further decreasing either T_{homo} or T_{het} could not obtain the film deposition at this concentration.

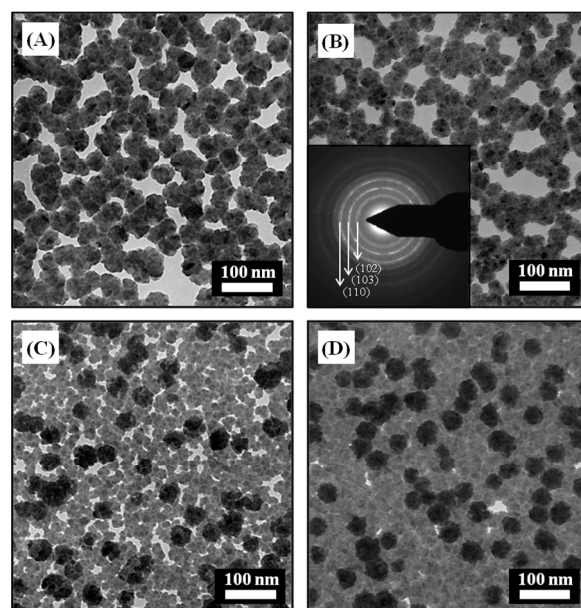


Fig. 3. TEM micrographs of Cu_xS films from heterogeneous reaction at $T_{\text{homo}} = 40\text{ }^\circ\text{C}$, $T_{\text{het}} = 40\text{ }^\circ\text{C}$, and at the residence times of 125 s for the deposition times of (A) 10 s (Entry 4), (B) 30 s (Entry 5), (C) 50 s (Entry 6), and (D) 75 s (Entry 7). The inset image in Fig. 3(B) shows electron diffraction pattern of the film.

Therefore, the concentration of reactants was further decreased to 5 times lower (Entries 8 ~ 10). T_{homo} and T_{het} were kept at room temperature ($\sim 25\text{ }^\circ\text{C}$) and at $80\text{ }^\circ\text{C}$, respectively, and the residence time of 62 s used for this deposition condition. At this condition, there is no evidence of particle formation from the homogeneous reaction, as shown in Fig. 4. Employing this particle-free flux condition, the Cu_xS film growth was then focused on the heterogeneous surface reaction. Fig. 4(A-C) illustrates TEM images collected from the heterogeneous reaction from different deposition times; (A) 10 s (Entry 8), (B) 20 s (Entry 9), and (C) 30 s (Entry 10), respectively. The film shows a higher coverage with an increase in the deposition. A cross-sectional SEM image of Cu_xS thin film prepared at deposition time of 120 s (Entry 22) is present in Fig. 4(D). It clearly shows that the film is smooth and continuous with the film thickness of $\sim 130\text{ nm}$. In addition, the insert image in Fig. 4(D) shows a corresponding surface morphology of the film.

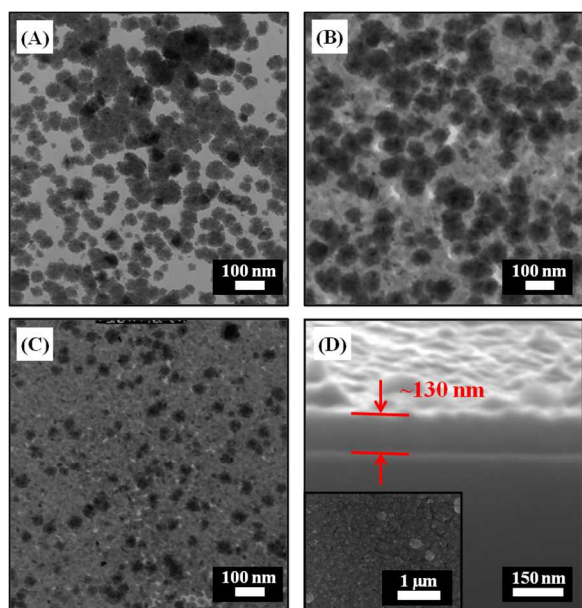


Fig. 4. TEM micrographs of Cu_xS films from heterogeneous reaction at $T_{\text{homo}} = 25\text{ }^\circ\text{C}$, $T_{\text{het}} = 80\text{ }^\circ\text{C}$, at the residence times of 62 s for the deposition times of (A) 10 s (Entry 8), (B) 20 s (Entry 9), and (C) 30 s (Entry 10). (D) A cross-sectional SEM image of Cu_xS thin film deposited at $T_{\text{homo}} = 25\text{ }^\circ\text{C}$, $T_{\text{het}} = 80\text{ }^\circ\text{C}$, residence time of 62 s, and deposition time of 120 s (Entry 22). The inset image in Fig. 4(D) shows a surface morphology.

Investigation of Cu_xS film growth under different growth conditions

Subsequently, the influence of the residence time on the film growth was studied *via* QCM measurement. The effect of different residence times of 62 s (Entry 11), 84 s (Entry 12), and 125 s (Entry 13) on Cu_xS film thickness are shown in Fig. 5. As expected, longer residence time (125 s) leads to higher growth rate ($\sim 0.66\text{ }\mu\text{m hr}^{-1}$, which was determined from the slope of the linear plot).

Fig. 6 shows the thickness of Cu_xS thin-film *vs.* the deposition time at different T_{homo} (25 $^\circ\text{C}$, 30 $^\circ\text{C}$, and 40 $^\circ\text{C}$) and T_{het} was kept constant at 40 $^\circ\text{C}$ with the residence time of 125 s (Entries 14 - 16). The results indicate that the initial growth rate as well as film thickness increases linearly, but there is limited influence on the growth rate of Cu_xS thin films with increasing T_{homo} .

Next, T_{homo} and residence time were kept at 25 $^\circ\text{C}$ and 62 s, respectively, and the effect of T_{het} on film growths were investigated (Entries 17 - 20). Fig. 7(A) shows the growth rate variation with the T_{het} from 60 $^\circ\text{C}$ to 90 $^\circ\text{C}$. The growth rate of 0.124, 0.272, 0.360, and 1.205 $\mu\text{m hr}^{-1}$ were obtained at the T_{het} of 60 $^\circ\text{C}$ (Entry 17), 70 $^\circ\text{C}$ (Entry 18), 80 $^\circ\text{C}$ (Entry 19), and 90 $^\circ\text{C}$ (Entry 20), respectively. This obviously shows the growth rates strongly depend on the T_{het} and are 40 - 100 times higher than that of deposited by CBD ($\sim 0.009\text{ }\mu\text{m hr}^{-1}$).¹⁸

The variation in growth rate is attributed only to the rate constant dependence on temperature, which can be expressed by Arrhenius equation

$$r(T) = A' \exp(-E_a/RT) \quad (6)$$

where $r(T)$ is the growth rate as a function of temperature, A' is the pre-exponential factor which includes the frequency factor and a constant related to the initial reagent concentration, E_a is the activation energy, and R is the molar gas constant. Fig. 7(B) represents the Neperian logarithm of the growth rate as a function of $1000/T$ (K), showing the linear dependence of temperature. E_a was determined from the slope of the linear fit of the logarithm of the growth rate as a function of $1000/T$ and is about 86 kJ mol^{-1} over the temperature range considered. This high value of E_a could be attributed to the combination of the hydrolysis of thiourea and the reaction of the rate limiting step for Cu_xS thin film formation.

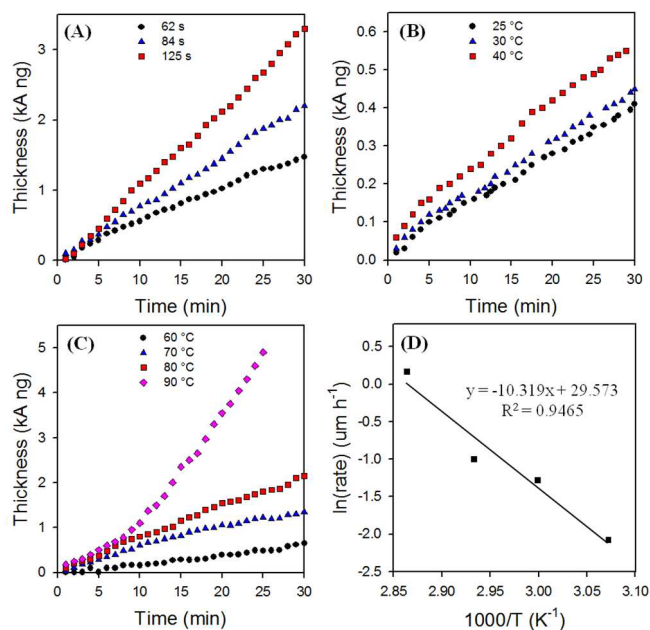


Fig. 5. QCM growth curves of Cu_xS thin films deposited (A) at the residence time of 62 s (Entry 11), 84 s (Entry 12), and 125 s (Entry 13); (B) at different T_{homo} of 25 $^\circ\text{C}$ (Entry 14), 30 $^\circ\text{C}$ (Entry 15), and 40 $^\circ\text{C}$ (Entry 16); (C) at different T_{het} of 60 $^\circ\text{C}$ (Entry 17), 70 $^\circ\text{C}$ (Entry 18), 80 $^\circ\text{C}$ (Entry 19), and 90 $^\circ\text{C}$ (Entry 20); (D) Neperian logarithm of the growth rate against $1000/T$ (K^{-1}).

The optical properties of the Cu_xS thin films were measured using a UV-Vis-NIR spectrophotometer. Absorption and transmission spectra of the Cu_xS films on glass substrate prepared by MASD, with durations of deposition ranging from 60 s - 240 s, are shown in Fig. 10(A) (Entries 21 ~ 23). All samples show NIR absorption due to surface plasmon effect.³⁷ The absorption band gradually increases in intensity with increasing the film thickness, which is attributed to the increasing density of generated copper vacancies.³⁸ This result indicates that the control of the parameter such as deposition time in MASD process could allow dynamic tuning of the atomic ratios and vacancy densities. The film deposited for 60 s (Entry 21) shows high transmittance in the visible region and lower transmittance towards the NIR region. The film visually

looks uniform and transparent with a metallic appearance (see the inset in Fig. 6(C)).

The optical band gaps (E_g) of the Cu_xS films were estimated from extrapolating the linear region of a plot of the squared absorbance versus the photon energy. Fig. 6(B) shows that the band gaps of the Cu_xS thin films in the range of 2.1 eV - 2.5 eV were obtained at 60 s - 240 s of deposition times, indicating different stoichiometry.²² Table 2 summarizes the Cu:S atomic ratio of Cu_xS films, average film thickness, and optical band gap, obtained at different deposition times. A trend of decreasing E_g with the increasing film thickness was observed at longer deposition time, leading to the lower sulphur content. EDS results show that the chemical composition is between $\text{Cu}_{1.10}\text{S}$ and $\text{Cu}_{1.15}\text{S}$, close to that of the stoichiometric covellite phase. It was also observed that the absorption edge of the films after annealing shifts to a shorter wavelength, which suggests a decrease in the band gap value because of low defect at high temperature.³⁹

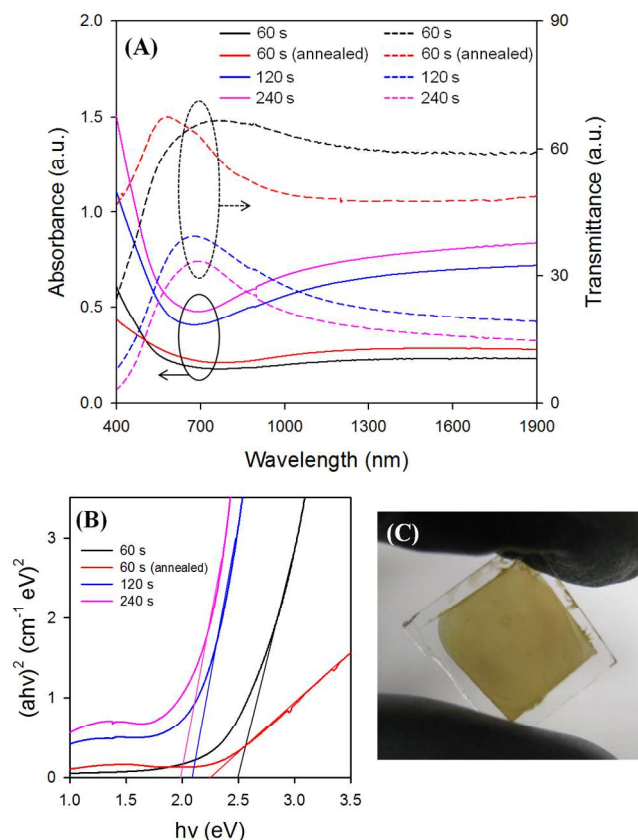


Fig. 6. (A) Optical absorption (solid) and transmission (dotted) spectra of Cu_xS films prepared at 60 - 240 s of deposition time. (B) Estimated band gap from the optical absorption spectra of Cu_xS films. (C) Film appearance deposited at 60 s (Entry 21).

Table 2. Influence of deposition time on the atomic ratio, film thickness, and band gap of Cu_xS films

Deposition time (sec)	Atomic ratio (Cu:S) ^a	Film thickness (nm) ^b	Band gap (eV) ^c	Entries
60	1:1.15 (1:1.10) ^d	115	2.5 (2.25) ^d	21
120	1:1.13	130	2.2	22
240	1:1.11	163	2.1	23

^a Measured by EDS. ^b Obtained from cross-sectional image of SEM. ^c Determined by extrapolating the linear region of a plot of the squared absorbance versus the photon energy. ^d Annealed film at 120 °C for 6 hrs under vacuum.

As-prepared film (Entry 21) was subsequently characterized by XRD technique in order to confirm the crystalline nature of the film. The XRD pattern does not show any diffraction peaks (Fig. 7(A)), indicating amorphous structure (or nanocrystalline) because the deposition procedure was performed at a low temperature. On the contrary, the annealed film showed peaks and could be indexed as the hexagonal covellite CuS phase (JCPDS No. : 06-0464). Therefore, amorphous CuS that is in a metastable phase was changed to the crystalline CuS which is thermodynamically more stable.³⁴

Raman spectroscopy is an ideal tool to identify the thin films as well as to quantify crystalline quality, even more so since XRD was not able to definitively identify the as-deposited Cu_xS film. Fig. 7(B) shows a strong band located at $\sim 472 \text{ cm}^{-1}$ which is assigned to the S-S stretching mode indicating the covellite CuS phase.^{21,41} Note that the peak observed for the annealed CuS film is stronger than the corresponding peak of the as-deposited Cu_xS film, indicating increased crystallinity, and a phase change was not observed.

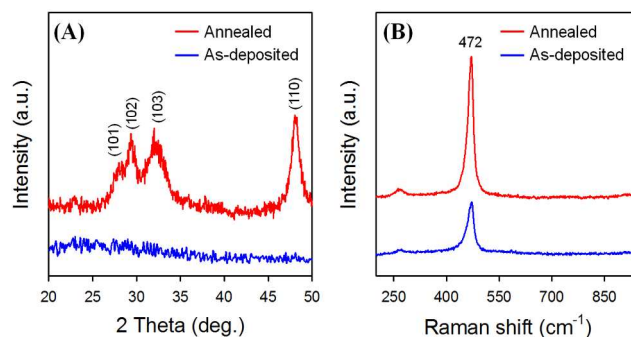


Fig. 7. (A) XRD patterns and (B) Raman spectra of before and after annealing the Cu_xS film deposited on glass substrate with conditions of Entry 21.

XPS was used to understand the structural changes of Cu_xS before and after annealing because the chemical or physical environment may affect the valence states of the films used in device fabrication and/or application. In each case of the Cu_xS film, the S 2p spectra have been fitted with doublets, the components of which have an intensity ratio of 2:1 for $2p_3$ to $2p_1$ and a separation of 1.2 eV (Fig. 8(A)). Both

as-deposited and annealed Cu_xS film revealed the presence of two well-defined doublets and a weak doublet at a higher binding energy, indicating the presence of two different binding states of sulfur in the samples (Fig. 8(A)). As-deposited Cu_xS film could be fitted to covellitic character at 161.1 eV and 162.2 eV, but it is difficult to understand their structural properties and limited in this study. One possible explanation for the high energy component in the sulfur XPS spectrum is that the presence of H bonded to S such as HS- would increase the S binding energy.⁴² The binding energies of the S $2p_3$ peak for the annealed Cu_xS film were 161.1 and 161.8 eV, which agreed well with the S $2p_3$ binding energies reported for sulfur in covellite CuS .⁴³

The XPS Cu $2p$ spectra of the samples are shown in Fig. 8(B). Peak fittings of the Cu $2p_3$ and Cu $2p_1$ spectra for both as-deposited and annealed Cu_xS film revealed the presence of two peaks that indicated the presence of two binding states of Cu at 932.8 eV and 933.8 eV, which are attributed to the Cu^{+1} and Cu^{+2} states, respectively.⁴⁴ The satellite feature at ~945 eV are evident of the Cu^{+2} in covellite CuS ,⁴⁴⁻⁴⁶ which is in good agreement with that of XRD and Raman results. The peak at 933.8 eV related with oxidized sulphide shifted after annealing the Cu_xS film by 0.8 eV, indicating reduced the amount of oxygen on the film surface.⁴⁷ The presence of oxidized species on as-deposited Cu_xS film could be attributed to all processes proceed in an open medium, therefore it is not possible to avoid ambient effect such as oxygen and water. As a result, as-deposited Cu_xS film can be described as amorphous covellitic CuS with volatile oxidized surface, which can be removed by simple annealing, and finally formed to the thermodynamically stable covellite CuS film.

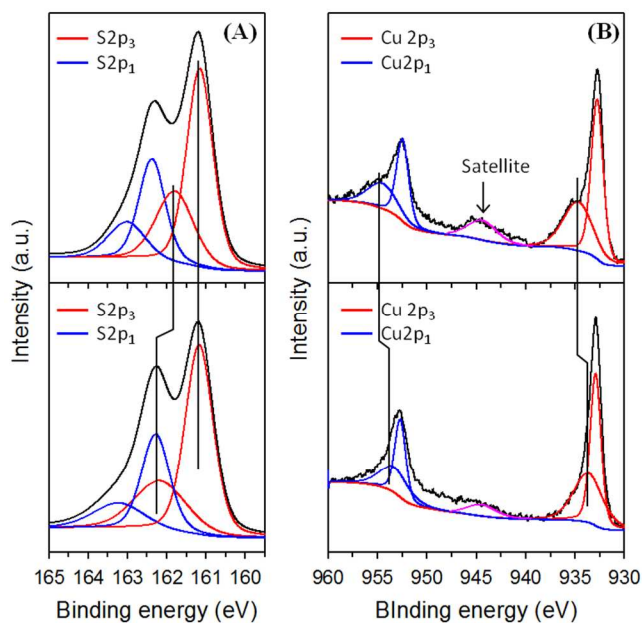


Fig. 8. (A) S $2p$ and (B) Cu $2p$ XPS spectra of (bottom) before and (top) after annealing the Cu_xS film deposited on glass substrate with conditions of Entry 21.

Based on the experimental results and our understanding, herein the growth kinetics and growth mechanism of covellite CuS thin film in the MASD process is presented. In order to determine the heterogeneous formation mechanism of Cu_xS thin films on the substrate, it is needed to consider a dominant sulfide source as it is responsible for Cu_xS thin film formation. One issue that was observed during the deposition where the short residence time condition was applied is that the Cu_xS film growth rate was very low so that there was no obvious Cu_xS thin film formed on the substrate, even if the thiourea concentration was still high. For example, when the Entries 4 - 7 conditions was applied for the film formation, the minimum residence time cannot be less than 125 s. As well as when the concentration is 2 times lower (Entries 8 - 10), the minimum residence time for Cu_xS film to form cannot be less than 62 s. It is possible that the dominant sulfide source that is involved in the Cu_xS thin film grown by MASD process may not be thiourea itself like what is generally proposed in the CBD mechanism but actually HS^- or S^{2-} ions.³² According to the thiourea hydrolysis reactions (see Eqs. 7 - 8), at pH = 10, most of the sulfide ions are in the form of HS^- rather than S^{2-} ($[\text{S}^{2-}] = 10^{-3.3}[\text{HS}^-][\text{OH}^-] = 10^{-7.3}[\text{HS}^-]$). Therefore, the main sulfide ions in the solution will likely be HS^- .



The possible explanation of the condition in which the growth rate is very low is that the concentration of HS^- , which is the dominant sulfide source, is very low at short residence times because the time is insufficient for thiourea to complete the hydrolysis process. This results in a very low growth rate of Cu_xS thin film deposition. Increasing residence time helps induce the hydrolysis of thiourea which achieves higher concentration of HS^- as well as S^{2-} . This behavior was found and explained before by Chang *et al.* of the CdS thin film deposition by continuous flow reactor process.³² They investigated the presence of dominant sulfide source by alternatively premixing thiourea with NH_4OH together in a stream, whereas the original recipe consists of NH_4OH in the same stream with Cd source. Sulfide ions in the form of HS^- from the thiourea hydrolysis reaction form in the stream rather than S^{2-} when the solution was maintained at pH 11 and at room temperature. The experimental results show that the deposited CdS thin films had a growth rate of about 2.5 times higher than that of the film using the original recipe. This result indicates that high concentration of sulfide ion in the premixed solution resulted in a higher growth rate of CdS thin film formation.

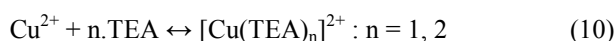
According to this finding, these kinetic insights could not be found by a conventional CBD process because all the reactants were sequentially put into the same solution bath and mixed all at once. By employing the developed MASD system, it enabled us to understand more in the fundamentals of Cu_xS film growth and also to control the mixing elements

and deposition conditions that cannot be operated by CBD. Therefore, the term of thiourea concentration present in the Cu_xS film growth mechanism in the following section needs to be HS^- concentration.

Due to a separate control of homogeneous reaction and heterogeneous reaction, the mechanisms of molecular level heterogeneous surface reaction and homogeneous particle formation tend to undergo different pathways. The HS^- ions formed through the thiourea hydrolysis reaction are the dominant sulfide source responsible for Cu_xS thin film formation. Free sulfide ions, S^{2-} then formed through an equilibrium hydrolysis reaction. For a homogeneous reaction, free copper ions, Cu^{2+} , are produced through a dissociation reaction of copper sulfate.



Copper ions are then complexed with TEA. The growth phase is suppressed by reducing the availability of free Cu^{2+} ions through the formation of the additional equilibrium:



Ammonium hydroxide is added to make an alkaline solution. The equilibrium in Eq. 11 provides ammonia and hydroxide ions in the solution.



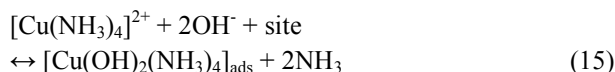
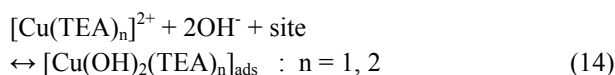
Free copper ions react with hydroxide ions to form the colloidal copper hydroxide in the bulk solution.



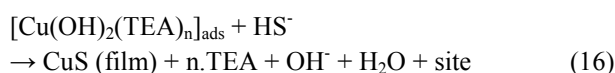
Colloids of $\text{Cu}(\text{OH})_2$ react with free sulfide ions, S^{2-} , and convert into CuS particles dispersed in the solution.



For the heterogeneous reaction on the substrate surface, the concentration of free copper ions is controlled by the formation of the complex equilibrium of both TEA and ammonia. When different complexing agents are present, the simultaneous presence of different complex ions is recognized.



The adsorbed dihydroxo-di(TEA)-copper and dihydroxo-diammino-copper react with dominant HS^- ions to generate copper sulfide. The site generation of covellite CuS thin films can be presented as Eqs.16 - 17.

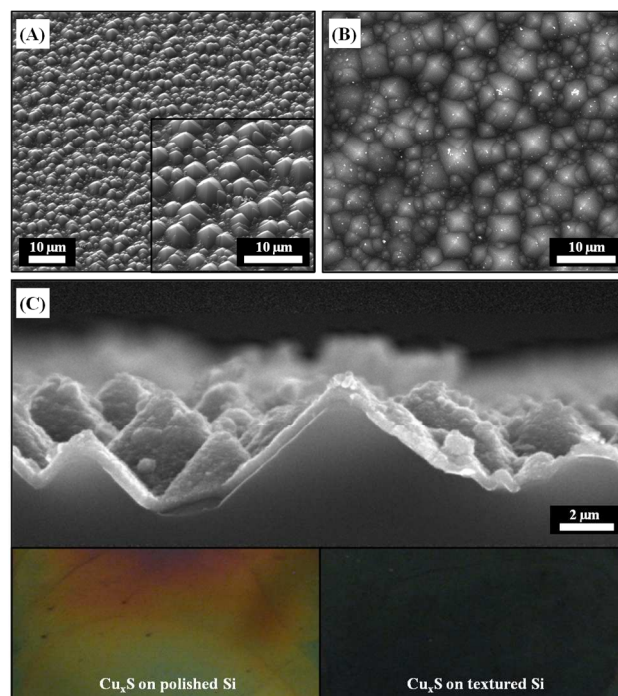


Two processes through the complexes of Cu^{2+} -TEA and Cu^{2+} - NH_3 are believed to occur simultaneously and Eqs. 16 - 17 are an important rate determining film growth step.

Conformal growth of Cu_xS films on textured surface for enhanced photon absorption

Conformal Cu_xS thin films were grown on top of smooth and textured Si surface using the MASD process to demonstrate its utility by measuring the reflections. Effective antireflection and light trapping characteristics within the absorbing material could achieve the high efficient solar cells using a textured substrate without the high cost of wafer fabrication.^{48,49} The textured Si surface was obtained by following the established method,⁵⁰ and the deposition condition is followed by Entry 21.

The resulting textured surface shown in Fig. 9(A) has various sizes of pyramidal shapes with approximately 1 - 3 μm per side at the base and about 1 - 2 μm high. Furthermore, the relatively uniform surface morphology of the as-deposited Cu_xS film was observed on textured pyramidal Si surface in Fig. 9(B) and the cross-sectional image in Fig. 9(C), and the Cu_xS film fully covers the surface with a thickness of about 200 nm, showing a conformal coverage.



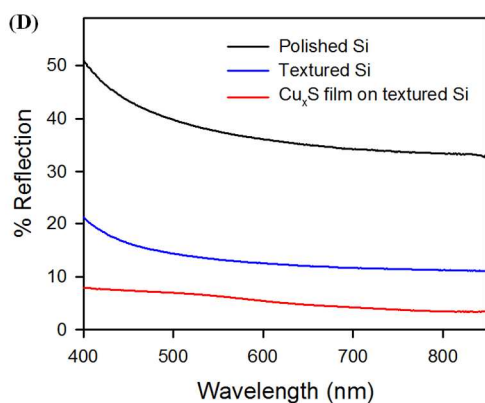


Fig. 9. (A) SEM image of a pyramidally textured Si surface (Inset shows a magnified image). (B) Top and (C) cross-sectional images of Cu_xS thin film on pyramidal Si surface deposited by MASD (Entry 21). The inset image in (C) show the appearance of Cu_xS films on polished Si (left) and on textured Si (right). (D) Comparison of the reflectance spectra of polished Si, pyramidally textured Si, and Cu_xS film on pyramidally textured Si surface.

The reflections for the polished Si, textured Si, and Cu_xS film on textured Si substrates were measured by UV-Vis spectrophotometer in an integrating sphere (Fig. 9(D)). The results show that the polished Si has a highly reflective surface with more than 35 % of visible light reflecting off, which is reduced to about 15 % on a textured Si surface in the range from 400 nm 900 nm. The inset image of Fig. 9(C) also demonstrates the comparison appearance of Cu_xS thin films on polished and textured pyramidal Si surfaces. It can clearly be seen that the reflectance of Cu_xS deposited on textured Si surface is much less than that of polished Si surface. Thus, MASD process is capable of depositing dense, conformal Cu_xS thin films uniformly on textured substrates.

Conclusion

We have demonstrated the optimum conditions for particle-free flux to promote molecule-by-molecule heterogeneous amorphous Cu_xS film growth by controlling the key parameters; concentration of mixed reactants, homogeneous temperature, heterogeneous temperature, and residence time in MASD system. This MASD system offers the way to separate the competing reactions of the homogeneous particle formation and thin film deposition from the molecular level heterogeneous surface reaction. The mixed reactant concentration can be decreased to 5 times lower than that of CBD, and the growth rate of resulting Cu_xS thin films deposited by MASD can be 40 - 100 times higher than that of deposited by CBD. The effects of these parameters were investigated by *in-situ* measurement to explain the influence on the kinetic growth of Cu_xS thin films. Based on the known properties of covellite CuS phase, the growth mechanism of Cu_xS thin films was proposed. The as-deposited covellitic Cu_xS film could simply be turned into a more crystalline structure by thermal annealing. Furthermore, MASD appears to be suitable technique to deposit high quality conformal Cu_xS thin films on textured surface that could provide an

economical throughput for fabricating thin absorber layers of solar cells.

Acknowledgements

P. Vas-Ummuay and K.-J. Kim contributed equally to this work. This research was supported by the DGIST R&D Programs of the Ministry of Education, Science and Technology of Korea (14-BD-05). The authors would like to thank Peter B. Kreider for XRD analysis and Pan Changqing for Raman analysis.

Notes and references

^aSchool of Chemical, Biological & Environmental Engineering, Oregon State University, Corvallis, OR 97331, United States, E-mail: Chih-hung.chang@oregonstate.edu

^bGreen Energy Research Division, Daegu Gyeongbuk Institute of Science & Technology, Daegu 711-873, South Korea

^cDepartment of Chemical Engineering, Faculty of Engineering, Chulalongkorn University 254 Payathai Road, Pathumwan Bangkok, 10330, Thailand

1. L. Tsakalakos, J. Balch, J. Fronheiser, B. A. Korevaar, O. Sulima and J. Rand, *Appl. Phys. Lett.*, 2007, **91**, 233117.
2. M. D. Kelzenberg, S. W. Boettcher, J. A. Petykiewicz, D. B. Turner-Evans, M. C. Putnam, E. L. Warren, J. M. Spurgeon, R. M. Briggs, N. S. Lewis and H. A. Atwater, *Nat. Mater.*, 2010, **9**, 239-244.
3. E. Garnett and P. Yang, *Nano Lett.*, 2010, **10**, 1082-1087.
4. S. Jeong, L. Hu, H. R. Lee, E. Garnett, J. W. Choi and Yi Cui, *Nano Lett.*, 2010, **10**, 2989-2994.
5. K. Ernst, A. Belaidi and R. Könenkamp, *Semicond. Sci. Technol.*, 2003, **18**, 475.
6. C. Lévy-Clément, R. Tena-Zaera, M. A. Ryan, A. Katty and G. Hodes, *Adv. Mat.*, 2005, **17**, 1512-1515.
7. H. Y. He, *Optoelectron. Adv. Mat.*, 2011, **5**, 1301-1306.
8. P. K. Nair, M. T. S. Nair, A. Fernandez and M. Ocampo, *J. Phys. D Appl. Phys.*, 1989, **22**, 829-836.
9. M. T. S. Nair and P. K. Nair, *Semicond. Sci. Tech.*, 1989, **4**, 191-199.
10. K. D. Yuan, J. J. Wu, M. L. Liu, L. L. Zhang, F. F. Xu, L. D. Chen and F. Q. Huang, *Appl. Phys. Lett.*, 2008, **93**, 132106.
11. L. Isac, A. Duta, A. Kriza, S. Manolache and M. Nanu, *Thin Solid Films*, 2007, **515**, 5755-5758.
12. A. Bollero, M. Grossberg, B. Asenjo and M. T. Gutierrez, *Surf. Coat. Tech.*, 2009, **204**, 593-600.
13. S. U. Offiah, P. E. Ugwoke, A. B. C. Ekwealor, S. C. Ezugwu, R. U. Osuji and F. I. Ezema, *Digest J. Nanomater. Bios.*, 2012, **7**, 165-173.
14. Y. Cao, M. S. Denny, Jr., J. V. Caspar, W. E. Farneth, Q. Guo, A. S. Ionkin, L. K. Johnson, M. Lu, I. Malajovich, D. Radu, H. D. Rosenfeld, K. R. Choudhury and W. Wu, *J. Am. Chem. Soc.*, 2012, **134**, 15644-15647.
15. P. Kumar and R. Nagarajan, *Inorg. Chem.*, 2011, **50**, 9204-9206.
16. Y. X. Zhao, H. C. Pan, Y. B. Lou, X. F. Qiu, J. J. Zhu and C. Burda, *J. Am. Chem. Soc.*, 2009, **131**, 4253-4261.
17. P. K. Nair, M. T. S. Nair, V. M. Garcia, O. L. Arenas, Y. Pena, A. Castillo, I. T. Ayala, O. Gomezdaza, A. Sanchez, J. Campos, H. Hu,

- R. Suarez and M. E. Rincon, *Solar Energy Mater. Solar Cells*, 1998, **52**, 313-344.
18. T.-Y. Ding, M.-S. Wang, S.-P. Guo, G.-C. Guo and J.-S. Huang, *Mater. Lett.*, 2008, **62**, 4529-4531.
19. R. S. Mane and C. D. Lokhande, *Mater. Chem. Phys.*, 2000, **65**, 1-31.
20. A. L. Abdelhady, K. Ramasamy, M. A. Malik, P. O'Brien, S. J. Haigh and J. Raftery, *J. Mater. Chem.*, 2011, **21**, 17888-17895.
21. S. D. Sartale and C. D. Lokhande, *Mater. Chem. Phys.*, 2000, **65**, 63-67.
22. J. Podder, R. Kobayashi and M. Ichimura, *Thin Solid Films*, 2005, **472**, 71-75.
23. Y. Xie, A. Riedinger, M. Prato, A. Casu, A. Genovese, P. Guardia, S. Sottini, C. Sangregorio, K. Miszta, S. Ghosh, T. Pellegrino and L. Manna, *J. Am. Chem. Soc.*, 2013, **135**, 17630-17637.
24. X. Li, A. Tang, L. Guan, H. Ye, Y. Hou, G. Dong, Z. Yang and F. Teng, *RSC Adv.*, 2014, **4**, 54547-54553.
25. S. He, G.-S. Wang, C. Lu, X. Luo, B. Wen, L. Guo and M.-S. Cao, *ChemPlusChem*, 2013, **78**, 250-258.
26. Y.-Z. Wei, G.-S. Wang, Y. Wu, Y.-H. Yue, J.-T. Wu, C. Lu and L. Guo, *J. Mater. Chem. A*, 2014, **2**, 5516-5524.
27. X.-J. Zhang, G.-S. Wang, Y.-Z. Wei, L. Guo and M.-S. Gao, *J. Mater. Chem. A*, 2013, **1**, 12115-12122.
28. S. He, G.-S. Wang, C. Liu, J. Liu, B. Wen, H. Liu, L. Guo and M.-S. Gao, *J. Mater. Chem. A*, 2013, **1**, 4685-4692.
29. K. M. Gadave and C. D. Lokhande, *Thin Solid Films*, 1993, **229**, 1-4.
30. Y. J. Lu, X. Meng, G. W. Yi and J. H. Jia, *J. Colloid Interf. Sci.*, 2011, **356**, 726-733.
31. P. Vas-Umuay and C.-H. Chang, *ECS J. Solid State Sci. Technol.*, 2013, **2**, P120-P129.
32. Y. J. Chang, Y. W. Su, D. H. Lee, S. O. Ryu and C. H. Chang, *Electrochem. Solid. St.*, 2009, **12**, H244-H247.
33. D. S. Boyle, A. Bayer, M. R. Heinrich, O. Robbe and P. O'Brien, *Thin Solid Films*, 2000, **361**, 150-154.
34. B. K. Paul, C. L. Hires, Y. W. Su, C. H. Chang, S. Rarnprasad and D. Palo, *Cryst. Growth Des.*, 2012, **12**, 5320-5328.
35. Y. J. Chang, P. H. Mugdur, S. Y. Han, A. A. Morrone, S. O. Ryu, T. J. Lee and C. H. Chang, *Electrochem. Solid. St.*, 2006, **9**, G174-G177.
36. P. H. Mugdur, Y. J. Chang, S. Y. Han, Y. W. Su, A. A. Morrone, S. O. Ryu, T. J. Lee and C. H. Chang, *J. Electrochem. Soc.*, 2007, **154**, D482-D488.
37. Y. Wu, C. Wadia, W. Ma, B. Sadtler and A. P. Alivisatos, *Nano lett.*, 2008, **8**, 2551-2555.
38. J. M. Luther, P. K. Jain, T. Ewers and A. P. Alivisatos, *Nat. Mater.*, 2011, **10**, 361-366.
39. F. E. Ghodsi, F. Z. Tepehan and G. G. Tepehan, *Surf. Sci.*, 2007, **601**, 4497-4501.
40. Y. Guo, J. Zhang, L. Yang, H. Wang, F. Wang and Z. Zheng, *Chem. Commun.*, 2010, **46**, 3493-3495.
41. N. R. deTacconi, K. Rajeshwar and R. O. Lezna, *J. Phys. Chem.*, 1996, **100**, 18234-18239.
42. R. A. D. Patrick, J. F. W. Mosselmans, J. M. Charnock, K. E. R. England, G. R. Helz, C. D. Garner and D. J. Vaughan, *Geochim. Cosmochim. Acta*, 1997, **61**, 2023-2036.
43. M. Kundu, T. Hasegawa, K. Terabe, K. Yamamoto and M. Aono, *Sci. Technol. Adv. Mater.*, 2008, **9**, 035011.
44. C. C. Chusuei, M. A. Brookshier and D. W. Goodman, *Langmuir*, 1999, **15**, 2806-2808.
45. H. Ye, A. Tang, C. Yang, K. Li, Y. Hou, F. Teng, *CrystEngComm*, 2014, **16**, 8684-8690.
46. W.-L. Sun, J. Xia and Y.-C. Shan, *Chem. Eng. J.*, 2014, **250**, 119-127.
47. V. Krylova and M. Andrulevicius, *Int. J. Photoenergy*, 2009, **2009**, 1-8 (Article ID 304308).
48. R. Dewan, M. Marinkovic, R. Noriega, S. Phadke, A. Salleo and D. Knipp, *Opt. Express*, 2009, **17**, 23058-23056.
49. R. Dewan, I. Vasilev, V. Jovanov and D. Knipp, *J. Appl. Phys.*, 2011, **110**, 013101.
50. C. W. Teplin, B. G. Lee, T. R. Fanning, J. Wang, S. Grover, F. Hasoon, R. Bauer, J. Bornstein, P. Schroeter and H. M. Branz, *Energy Environ. Sci.*, 2012, **5**, 8193-8198.